

Durham Research Online

Deposited in DRO:

14 June 2017

Version of attached file:

Accepted Version

Peer-review status of attached file:

Peer-reviewed

Citation for published item:

Cooper, George F. and Morgan, Daniel J. and Wilson, Colin J.N. (2017) 'Rapid assembly and rejuvenation of a large silicic magmatic system : insights from mineral diffusive profiles in the Kidnappers and Rocky Hill deposits, New Zealand.', *Earth and planetary science letters.*, 473 . pp. 1-13.

Further information on publisher's website:

<https://doi.org/10.1016/j.epsl.2017.05.036>

Publisher's copyright statement:

© 2017. This manuscript version is made available under the CC-BY-NC-ND 4.0 license
<http://creativecommons.org/licenses/by-nc-nd/4.0/>

Additional information:

Use policy

The full-text may be used and/or reproduced, and given to third parties in any format or medium, without prior permission or charge, for personal research or study, educational, or not-for-profit purposes provided that:

- a full bibliographic reference is made to the original source
- a [link](#) is made to the metadata record in DRO
- the full-text is not changed in any way

The full-text must not be sold in any format or medium without the formal permission of the copyright holders.

Please consult the [full DRO policy](#) for further details.

**Rapid assembly and rejuvenation of a large silicic magmatic
system: insights from mineral diffusive profiles in the Kidnappers
and Rocky Hill deposits, New Zealand**

George F. Cooper^{1*}, Daniel J. Morgan², Colin J.N. Wilson³

¹Department of Earth Sciences, Durham University, Science Labs, Durham DH1 3LE, UK

²School of Earth and Environment, The University of Leeds, Leeds LS2 9JT, UK

³School of Geography, Environment and Earth Sciences, Victoria University of Wellington,
P.O. Box 600, Wellington 6140, New Zealand

*corresponding author

email: george.cooper@durham.ac.uk

phone: +44 (0) 191 33 42356

Abstract

The timescales over which magmas in large silicic systems are reactivated, assembled and stored remains a fundamental question in volcanology. To address this question, we study timescales from Fe-Mg interdiffusion in orthopyroxenes and Ti diffusion in quartz from the caldera-forming 1200 km³ Kidnappers and 200 km³ Rocky Hill eruptions from the Mangakino volcanic centre (Taupo Volcanic Zone, New Zealand). The two eruptions came from the same source area, have indistinguishable ⁴⁰Ar/³⁹Ar ages (~1.0 Ma) and zircon U-Pb age spectra, but their respective deposits are separated by a short period of erosion. Compositions of pumice, glass and mineral species in the collective eruption deposits define multiple melt dominant bodies but indicate that these shared a common magmatic mush zone. Diffusion timescales from both eruptions are used to build on chemical and textural crystal signatures and interpret both the crystal growth histories and the timing of magma accumulation. Fe-Mg interdiffusion profiles in orthopyroxenes imply that the three melt-dominant bodies, established through extraction of melt and crystals from the common source, were generated within 600 years and with peak accumulation rates within 100 years of each eruption. In addition, a less-evolved melt interacted with the Kidnappers magma, beginning ~30 years prior to and peaking within 3 years of the eruption. This interaction did not directly trigger the eruption, but may have primed the magmatic system. Orthopyroxene crystals with the same zoning patterns from the Kidnappers and Rocky Hill pumices yield consistently different diffusion timescales, suggesting a time break between the eruptions of ~20 years (from core-rim zones) to ~10 years (outer rim zones). Diffusion of Ti in quartz reveals similarly short timescales and magmatic residence times of < 30 years, suggesting quartz is only recording the last period of crystallization within the final eruptible melt. Accumulation of the eruptible magma for these two, closely successive eruptions was accomplished over centuries to decades, in contrast to the gestation time of the magmatic system of ~200 kyr, as

indicated by zircon age patterns. The magmatic system was able to recover after the Kidnappers eruption in only ~10-20 years to accumulate enough eruptible melt and crystals for a second ~200 km³ eruption. Our data support concepts of large silicic systems being stored as long-lived crystal mushes, with eruptible melts generated over extraordinarily short timescales prior to eruption.

Keywords

Diffusion chronometry; Fe-Mg in orthopyroxene; Ti in quartz; magmatic timescales; supereruption; Taupo Volcanic Zone

1. Introduction

Establishing the timescales of magmatic processes associated with large explosive eruptions provides important insights into the dynamics of large-scale crustal magmatic systems and the processes that lead up to eruption. There are two contrasting, but complementary, approaches to measuring these time scales, both of which utilise mineral phases in the eruption products. The first involves direct age dating of crystallization events through such techniques as U-series or U-Pb dating of suitable accessory mineral phases, such as zircon, allanite, or titanite (e.g. Schmitt, 2011) or the use of parent-daughter isochrons, such as Rb/Sr techniques in feldspars (e.g. Davies et al., 1994). The second approach is that of indirect age dating through diffusion modelling of inferred step-changes in compositional characteristics in minerals (e.g. Costa et al., 2008; Chakraborty, 2008; Costa and Morgan, 2010). Rather than dating the age of crystals themselves, this approach measures the time elapsed at magmatic temperatures following periods of renewed growth and formation of crystal zonation within individual grains.

For those eruptive units where both of these approaches have been undertaken, there is an apparent contrast between the respective results. Crystal-specific ages indicate histories of typically 10^3 to $>10^5$ years, whereas diffusion modelling yields estimates in the 10^1 to 10^3 years range (e.g. Turner and Costa, 2007; Cooper and Kent, 2014). This contrast can be linked to the inference that the chemical processes leading to these magmas (and growth of their crystal cargo, particularly the zircons that are dated) can be prolonged and magma within large silicic systems may be stored at near-solidus conditions for long periods of time (Cooper and Kent, 2014). This concept involves the waxing and waning of a crystal-rich, melt-poor (mush) system and the generation of large volumes of melt of given composition through fractionation, controlled by the rates at which material and heat are added and heat can be lost (e.g. Hildreth, 2004; Bachmann and Bergantz, 2004). On the other hand, processes involved in the mobilisation and extraction of that melt into eruptible bodies can occur much more rapidly because they only involve the physical transportation of melt \pm crystals (Wilson and Charlier, 2009; Gualda et al., 2012; Allan et al., 2013; Barker et al., 2016).

The textures, compositions and thicknesses of growth zones within crystals can be used to discriminate between different magmatic processes responsible for the zonation (Saunders et al., 2012; Allan et al., 2013; Kahl et al., 2013). Each crystal interior may have a diverse and complex growth history, but zoning features that are common to a substantial proportion of all crystals allow for the distinction to be made between localised versus system-wide crystal histories. In the case of the Oruanui and post-Oruanui rhyolites from Taupo volcano the zoning in phenocryst phases records common magmatic histories and suggests rapid rejuvenation of crystal mushes and melt accumulation (Allan et al., 2013; Barker et al., 2016). In addition, there may be disparities in the timescales estimated from different phases recording seemingly common processes (e.g. Chamberlain et al., 2014) and so if zoning within the crystals permits, it is important to consider the timescales from

multiple phases. Here we present pre-eruptive timescales for assembly of the final erupted melt-dominant bodies inferred from Fe-Mg interdiffusion in orthopyroxene and Ti diffusion in quartz from pumices in two eruptions, the Kidnappers and Rocky Hill events from Mangakino volcanic centre, New Zealand (Tables 1 and 2). We also use the difference in timescales from common growth zones within orthopyroxenes from the Kidnappers and Rocky Hill deposits to constrain the time break, inferred from field evidence to be geologically short, between the two eruptions.

2. Kidnappers and Rocky Hill eruptions

The Kidnappers and Rocky Hill eruptions occurred from the Mangakino volcanic centre, a composite caldera system in the Taupo Volcanic Zone, New Zealand (Fig. 1; Wilson et al., 2009). The Kidnappers eruption ($\sim 1200 \text{ km}^3$ DRE) generated a large, fine-grained phreatomagmatic fall deposit (Carter et al., 2004; Cooper et al., 2012), followed by an exceptionally widespread, non-welded ignimbrite (Wilson et al., 1995). It was followed, after a short interval of erosion, by the $\sim 200 \text{ km}^3$ Rocky Hill eruption which mostly generated a partly-welded ignimbrite (Cooper et al., 2016). The two deposits yield identical $^{40}\text{Ar}/^{39}\text{Ar}$ ages within uncertainty at $\sim 1.0 \text{ Ma}$ (Wilson et al., 1995) and their zircon U-Pb age spectra are also closely similar, ranging back to between 100 and 200 kyr prior to the eruption age (Cooper et al., 2014).

Textural and compositional records from the major mineral phases (plagioclase, quartz, amphibole, orthopyroxene), coupled with thermobarometric model constraints suggest that both eruption deposits were sourced from a common magmatic system with crystals originating from a shared mush zone (Cooper et al., 2016). However, compositions of glass shards and glass-selvaged crystals from the fine grained Kidnappers fall deposit (Cooper et al., 2012) and pumices, matrix glass and crystal phases from the Kidnappers and Rocky Hill

ignimbrites (Cooper et al., 2016) show variations consistent with there being multiple discrete melt-dominant magma bodies tapped during the collective events. There are three distinguishable glass compositions in the Kidnappers fall deposit (KF-A, KF-B and KF-C), three pumice groups in the Kidnappers ignimbrite (KI-1, KI-2, KI-3), and two pumice groups in the Rocky Hill ignimbrite (RH-1, RH-2). Of these, modal abundances and glass and mineral chemistries link the two most voluminous as (i) KF-A = KI-1 = RH1 and (ii) KF-B = KI-2 = RH-2. The two other magma types are (iii) glass type KF-C, which forms a minor proportion of the Kidnappers fall deposit and is compositionally overlapped by glass from pumice type KI-1 and (iv) the lower silica pumice type KI-3 found only in the Kidnappers ignimbrite (see Cooper et al., 2016, for full descriptions).

Within the Kidnappers and Rocky Hill deposits, it is particularly relevant to identify compositional zones within crystals that record the same apparent processes in both eruptions, with the aim of assessing the differences in model timescales during the lead up to the respective eruptions. Orthopyroxene is the ideal choice within this system, as simple zoning patterns are present which, together with an extensive textural and geochemical dataset (Cooper et al., 2016), strongly suggest that orthopyroxene shares common growth histories with the other crystal phases. We compare the diffusive timescales from orthopyroxene with those from quartz in order to see if the crystal phases, from multiple magma bodies, are recording the same chamber-wide magmatic events.

3. Samples

Orthopyroxene and quartz crystals were picked from representative pumices from each of the compositional groups in the Kidnappers and Rocky Hill ignimbrites (Cooper et al., 2016). Kidnappers pumices were sampled from Litchfield Quarry ~30 km from source at NZMG grid reference 2758837m E, 6339943m N (Fig. 1). Diffusion profile determinations

were made from orthopyroxenes in Kidnappers samples P1655 and P17XX from KI-3; P1607, P1609, P2006 and P2015 from KI-1; and P1646, P1649 and P2011 from KI-2. Rocky Hill pumices were sampled from exposures in the Waipa Valley, ~50 km from source (Fig. 1). Diffusive age determinations were made from orthopyroxenes in Rocky Hill samples P2000, P2029, P2042, P2049 and P2050 from RH-1 and sample P2046 from RH-2. Ti-in-quartz diffusion ages were determined from one Kidnappers KI-2 pumice (P2006), the zircons in which were dated by U-Pb techniques (Cooper et al., 2014), and one Rocky Hill RH-1 pumice (P2050).

4. Methods

4.1. Measurement techniques

Orthopyroxene

Orthopyroxenes were orientated in epoxy blocks with the crystal (*a*- or *b*-) and *c*-axes exposed. High resolution backscattered electron (BSE) images of each orthopyroxene crystal were taken to investigate crystal zonation features and mark the location of individual analyses. Crystal cores, rims and any prominent zonation features (intermediate domains) were targeted for analysis by EPMA using a JEOL JXA-8230 Superprobe at Victoria University of Wellington. Crystals were analysed with a 15 kV accelerating voltage and a 12 nA focused beam. A strong negative linear relationship ($R^2 = 0.95$) was observed between BSE greyscale values and the Mg/(Mg+Fe) content of multiple orthopyroxene crystals, and therefore the zoning observed in BSE images was inferred to be an accurate reflection of the Fe-Mg content (Supplementary Fig. 1). This relationship allowed the gradients in Fe-Mg concentrations to be investigated at a higher spatial resolution than is possible from spot analyses alone (Morgan et al., 2004; Martin et al., 2008; Saunders et al., 2012; Allan et al., 2013). The software package *Image J* (<http://rsb.info.nih.gov/ij/>) was used to extract spatially

resolved profiles of BSE intensity across crystal zonation boundaries. The linear relationship between the Fe-Mg content of the orthopyroxenes and intensity of backscattering (greyscale value: Supplementary Fig. 1) was used to quantify Mg/(Mg+Fe) concentration gradients between the EPMA analytical spots on either side of the diffusion profile. It is assumed that the boundaries chosen for modelling initially had step-wise concentration gradients, which over time at magmatic temperatures were modified by Fe-Mg interdiffusion, and that diffusion ceased upon quenching on eruption, resulting in sigmoidal concentration gradients. Finite-difference software was used to generate a database of simulated sigmoidal diffusion profiles, which obey composition-dependent diffusion under a 1-D (linear) diffusion geometry; these were then adapted to the samples via application of scaling laws using Excel.

Dohmen et al. (2016) provided a new set of experimentally determined interdiffusion coefficients. However, this study only used highly magnesian compositions (En₉₁₋₉₈) that are well outside the compositional range of the Kidnappers/Rocky Hill orthopyroxenes (En₄₁₋₆₈). Therefore, to calculate orthopyroxene $D_{\text{Fe-Mg}}$ we employed the parameterization of Ganguly and Tazzoli (1994) who utilised compositions close to those of this study and also determined a more significant compositional dependence. Indeed, our observation of asymmetric diffusion profile shapes as a function of the composition dependence is completely consistent with the composition dependence proposed by Ganguly and Tazzoli (1994). In terms of oxygen fugacity, Dohmen et al. (2016) suggest a much lower $f\text{O}_2$ dependence than that found in olivine (exponent of $1/6$, e.g. Dohmen and Chakraborty, 2007). This result does contradict the value of oxygen fugacity dependence suggested (in the absence of experimental constraints) by Ganguly and Tazzoli (1994) based on analogy with olivine. We have therefore, for the purposes of this study, used the equation of Ganguly and Tazzoli (1994) but without an oxygen fugacity component.

Quartz

Cathodoluminescence (CL) imaging was used to show zoning within quartz grains, where the brightness of the image element is inferred to directly correspond to the Ti concentration (Wark et al., 2007; Matthews et al., 2012a, b). High-resolution CL images of Ti variations in quartz grains were obtained on a FEI Quanta 650 FEG-SEM (field emission gun—scanning electron microscope) with a KE Centaurus panchromatic CL detector at the University of Leeds.

Ti in quartz diffusivities can be calculated in the following way from the parameterisation of Cherniak et al. (2007):

$$D_{Ti} = D_{Ti,0} e^{\left(\frac{-E}{RT}\right)},$$

where $D_{Ti,0}$ is the D_0 for Ti ($7 \times 10^{-8} \text{ m}^2 \text{ s}^{-1}$), E is the activation energy ($273 \pm 12 \text{ kJ mol}^{-1}$), R is the gas constant ($8.314 \text{ J mol}^{-1} \text{ K}^{-1}$) and T is temperature (in Kelvin). Having calculated the appropriate values of D for each elemental system at the appropriate temperature, the following equation was solved for time (Crank, 1979; Morgan et al., 2004):

$$C = C_0 + \frac{(C_1 - C_0)}{2} \left[\operatorname{erfc} \left(\frac{x}{2\sqrt{D_i t}} \right) \right],$$

where C is the normalised concentration of Ti, C_0 and C_1 refer to the initial amounts of the element on each side of an initial interface, D_i is the calculated diffusivity in $\text{m}^2 \text{ s}^{-1}$, t is the diffusion time and x is the position measured in metres along the profile and centred on the interface (the mid-point of the profile). The difference between modelled profile shape and the input profile were minimised using an Excel macro to get a best-fit profile from which a model timescale could be calculated.

4.2. Parameters and uncertainties

It is essential to consider the sources and magnitude of uncertainties in diffusion modelling

(Chakraborty, 2008; Costa and Morgan, 2010). Calculations for $D_{\text{Fe-Mg}}$ are insensitive to pressure (Dohmen and Chakraborty, 2007), but highly sensitive to temperature (diffusion data of Besancon, 1981, and Schwandt et al., 1998). Here we adopt different magmatic temperatures for each compositional group within the Kidnappers and Rocky Hill (Table 1), based on estimates from measured amphibole rim compositions (Cooper et al., 2016) and using the model of Ridolfi et al. (2010: Table 1). Regardless of the model used to estimate absolute temperature values, the relative difference between compositional groups is always consistent (Cooper et al., 2016). Amphiboles used in this study have common final growth histories with orthopyroxenes (Cooper et al., 2016) and therefore temperatures estimated from amphibole rims are inferred to also represent the corresponding temperatures during orthopyroxene growth. Within the low-SiO₂ Kidnappers group (KI-3) a significant number of crystals have up-temperature rim signals and therefore a higher temperature (based on corresponding up-temperature amphibole rims) is adopted for this group. In the other compositional groups where down-temperature rim signals dominate, the temperature used is lower, yielding maximum age estimates. For uncertainty calculations on single model-age determinations, temperature uncertainties of ± 30 °C (1σ) were used, based on common thermometry uncertainties (Blundy and Cashman, 2008). It is possible that temperature fluctuated during the diffusion process, which would have the effect of shortening (higher temperatures) or lengthening (lower temperatures) the modelled timescales. However, there is no evidence from any crystal phase (e.g. oscillatory zoning) for a significant shift in temperature during diffusion of the modelled boundaries and therefore all modelled timescales in this study assume an isothermal history.

The uncertainties associated with profile shapes (i.e. the compositional integrity of the BSE images) and the profile lengths (based upon the absolute reliability of the magnification provided by microprobe imaging) were also taken into account, and a conservative value of

± 3 % was adopted as a maximum uncertainty on profile lengths. The validity of estimates based on crystal zonation boundaries that display sigmoidal profiles over short ($< \sim 5 \mu\text{m}$) length scales, implying very short timescales of ≤ 3 years at the conditions relevant to this study (Table 1), needs to be considered with caution. Such boundaries may reflect a tangible record of very short-lived processes in the magma, but may potentially also be an artifact of pixel size and effects of convolution in the BSE imaging and during image rotation steps or sampling of an image along an inclined traverse. Convolution can be particularly problematic where image pixel size is very small ($\sim 0.25 \mu\text{m}$) compared to the spatial resolution and excitation volume of the electron beam ($< 1 \mu\text{m}$), potentially smearing out a genuinely sharp stepwise boundary and generating an artificial diffusion profile (Morgan et al., 2004). To test for this effect, the resolution limit was estimated by taking a BSE profile across the edge of orthopyroxene crystals and into the glass selvage at different image magnifications and resolutions (Fig. 2). The lower magnification (x120) and resolution image shows a $\pm 1 \mu\text{m}$ smearing over the edge of the crystal (assumed to be a stepwise boundary). At higher magnification (x370) and resolution this effect is reduced to $\pm 0.25 \mu\text{m}$ (Fig. 2). These lengths are $\sim 12\%$ and $\sim 5\%$, respectively, of the measured diffusion profile lengths, and thus yield uncertainties that are considerably smaller than those associated with the temperature estimates. However, to account for possible convolution effects, the youngest ages (0-3 years) are grouped here as ' < 3 years'.

The finest-scale time scale resolution available for CL images of quartz was estimated by modelling a known sharp contact (crystal edge or crack). This yielded a timescale of 0.5 years (at 780°C), which is thus the shortest resolvable age via CL imaging. Any diffusion-based age estimates of < 0.5 years are thus unresolvable using CL imaging and are rejected. As with orthopyroxene, all timescales can be considered as maximum ages due to the assumption that the initial boundary had a step-wise concentration gradient. Changing this

assumption would only serve to shorten the timescales further.

5. Results

5.1. Textural characteristics of Kidnappers and Rocky Hill orthopyroxenes

The zoning within individual orthopyroxene crystals in the Kidnappers and Rocky Hill samples can be complex. There are, however, key overarching textural features that allow crystals to be classified into distinct populations (Table 1 and Supplementary Fig. 2). Four main orthopyroxene crystal populations (referred to here as normal, unzoned, reverse and patchy) are present, based on the simplified textural characteristics observed in BSE images. In addition, these populations can have a dark outer zone (within 100 μm of the outermost rim, or forming the outermost rim itself) that may overprint any of the above textures (Supplementary Fig. 2). Here, boundaries from both normal- and reverse-zoned grains are utilised for modelling. Grains with an overprinted dark outer zone (higher Mg#) are of particular interest for modelling timescales, as they are found in orthopyroxene crystals from both eruptions. Textures of plagioclase grains and the chemistry of amphiboles from the Kidnappers and Rocky Hill eruptions have features consistent with those of the orthopyroxenes and thus all these phases are inferred to share a common magmatic history for the modelled period of time prior to eruption (Cooper et al., 2016).

To assess both the primary zonation and diffusion-affected zonation, elemental mapping of selected crystals using EPMA was carried out (Supplementary Figs. 3, 4). In orthopyroxene, Al has a very slow diffusion rate, Ca is slow, and Fe and Mg have relatively fast diffusion rates (Sautter et al., 1988). Al can be considered to be effectively immobile over timescales of <10,000 years at the magmatic temperatures applicable to the Kidnappers/Rocky Hill system (Smith and Barron, 1991) and thus closely records the original growth zonation of the orthopyroxene. Blurring in Al content across boundaries parallel to the

c-axis is evident, which cannot realistically be attributed to diffusion. Therefore, we conclude that growth must have exerted a strong control parallel to the *c*-axis when compared to the sharper boundary along the *a*- or *b*-axes, which have negligible blurring, and, we infer, negligible growth effects to interfere with the diffusion profiles.

5.2. Fe-Mg diffusion timescales in Kidnappers and Rocky Hill orthopyroxenes

Within Kidnappers orthopyroxenes, timescales were modelled across the boundaries perpendicular to the *c*-axis both between cores and rims, and between intermediate domains and dark outer zones (the latter are common in the KI-3 compositional group). The corresponding boundaries were also modelled within Rocky Hill orthopyroxenes. Commonly, Rocky Hill grains display an additional, BSE-lighter outer rim overgrowing the dark outer zones, and therefore the additional intervening boundary was also modelled (Fig. 3). Core-rim boundaries cover a spectrum from those with very dark cores found in the interior of the crystal, to broader cores where the boundary is found towards the exterior of the crystal (Fig. 3). All modelled diffusion ages across the full range of core-rim boundaries were grouped together, as definite textural distinctions that may represent unique events are difficult to establish. All modelled boundaries were parallel to the *a*- or *b*-axes, which display concentration gradients that are consistent with diffusive modification (Supplementary Figs. 2, 3).

Modelled diffusion timescales from core-rim boundaries within the Kidnappers steadily increase in abundance from ~600-150 years, followed by a sharper increase within 150 years to a peak at ~20 years before eruption (Fig. 4). Modelled diffusion timescales from analogous core-rim boundaries within the Rocky Hill show a continuous increase in abundance from ~ 600 to 100 years, followed by a step change in gradient at <100 years to a peak ~ 40 years before eruption (Fig. 4). There is a ~20 year difference in peak PDF ages of

core-rim zones between the Kidnappers (~20 years) and the Rocky Hill (~40 years). Only three modelled boundaries across very dark cores from both eruptions return significantly older pre-eruptive ages (>600 years).

All dark exterior zones from Kidnappers orthopyroxenes were modelled from within the low-SiO₂ (KI-3) pumice group. The number of resulting time estimates range from 30 years to within one year of eruption, with a peak PDF age of ~3 years (Fig. 4). Notably fewer orthopyroxene grains with dark exterior zones are found within the Rocky Hill (Table 1). The grains displaying this texture in the Rocky Hill are inferred on compositional grounds to be inherited from the common mush zone originally tapped during the Kidnappers eruption (Cooper et al., 2016). Timescales from both the rim-side and core-side of dark exterior zones in the Rocky Hill extend back further than those from the Kidnappers. Modelled ages are between 240 and 10 years, and the PDF curve has a peak at ~13 years prior to eruption (Fig. 4). The peak PDF age difference between the dark outer zones of the Kidnappers (~3 years) and Rocky Hill (~13 years) is ~10 years by this methodology.

All Fe-Mg interdiffusion timescales presented here suggest older ages are less likely. This may be the result of an acceleration in the recorded process <100 years prior to eruption (cf. Allan et al., 2013). Alternatively, these trends may be the result of older boundaries being overwritten, settling and hence loss of older crystals, or dilution due to the magma volume increasing through time.

5.3. Textural characteristics of Kidnappers and Rocky Hill quartz

In Kidnappers and Rocky Hill pumices, quartz forms euhedral, bipyramidal, but often broken crystals up to ~2 mm across. CL imaging of quartz within the Kidnappers and Rocky Hill pumices reveals oscillatory and complexly zoned grains with the greyscale intensity inferred to reflect Ti concentrations (Wark et al., 2007; Matthews et al., 2012a, b; Fig. 5).

Oscillatory zoning is commonly truncated by (multiple) resorption surfaces and embayments are also common (Fig. 5). CL-imaged quartz crystals from the Kidnappers and Rocky Hill pumices were classified into three groups: (1) grains displaying darker rims (lower Ti) and (2) lighter rims (higher Ti), and (3) those with no significant compositional change at the rim (Table 2). Within a single KI-2 (high SiO₂) Kidnappers pumice, grains with darker rims (lower Ti) dominate over those with lighter rims (Table 2) and thus provide evidence of an apparent temperature decrease prior to eruption, consistent with the other mineral phases (Cooper et al., 2016). This down-temperature signal is interpreted to represent movement of the KI-2 magma to a shallower storage level prior to eruption (Cooper et al., 2016). In contrast, grains within a single Rocky Hill (RH-1) pumice are dominated by lighter (higher Ti) rims (in contrast to those with darker rims and those showing no change: Table 2), reflecting an increase in apparent temperatures during growth prior to eruption. The contrasting quartz histories reflect the multiple melt dominant bodies present in the Kidnappers/Rocky Hill magmatic system and are in accord with the corresponding orthopyroxene textural characteristics in the respective pumice types (Table 1).

5.4. Ti diffusion timescales in Kidnappers and Rocky Hill quartz

The complexity of the zoning within Kidnappers and Rocky Hill quartz did not allow for a distinctive zone common to all grains to be modelled, so therefore all zones which displayed a diffusive boundary were considered. Modelled Ti diffusion timescales across boundaries ranging from the core to rim of Kidnappers quartz are all within 31 years of eruption, with the exception of one at 130 yrs. The ages increase from 31 years to a peak at ~5 years before eruption (Fig. 6). Modelled Ti timescales from Rocky Hill quartz are all within 42 years of eruption and are very similar to the Kidnappers timescales. The ages peak at ~2

years prior to eruption (Fig. 6). The Ti-in-quartz timescales obtained are comparable to those from orthopyroxene, in particular, those from dark outer zones (Fig. 7).

6. Discussion

6.1. Implications of diffusion timescales from orthopyroxene dark exterior zones

Evidence from the presence of BSE-darker exterior zones in orthopyroxene grains, as well as the ‘up-temperature’ signals recorded in amphibole, plagioclase and matrix glass from the low-SiO₂ Kidnappers (KI-3) pumice group is taken to represent mixing with, or rejuvenation through interaction with, a less evolved and/or hotter melt (Fig. 8; Cooper et al., 2016). Modelled timescales across the interior domain to darker exterior zone boundary thus reflect the time (<50 yrs; Fig. 8) before eruption when this interaction occurred. Over the 50 year period, the number of crystal boundaries recording the interaction with the less-evolved melt increased within the KI-3 magma volume up to the point of eruption, within the limits of resolution of the imagery (PDF peak at <3 years; Fig. 4). The extent of interaction by the less-evolved melt thus progressively increased in the <50 years before eruption, and might be considered as a eruption triggering mechanism (cf. Wark et al., 2007). However, the proportion of material with these signatures of interaction with the less-evolved melt is relatively small (~3% of total erupted Kidnappers material). The magmatic rejuvenation therefore seems unlikely to have had a system-wide influence. We infer that interaction of the hotter and/or less evolved melt, possibly through underplating at the base of the mush column, essentially primed a volume of material for eruption through thermal rejuvenation and/or volatile exchange, rather than being the eruption trigger itself (cf. Chamberlain et al., 2014).

Geochemical and petrological evidence from Kidnappers and Rocky Hill deposits strongly suggests that both eruptions were derived from a common magmatic system (Cooper

et al., 2016). Consequently, orthopyroxene grains with a dark exterior zone (plus additional rim growth) in the Rocky Hill can be inferred to record the same processes as seen within the Kidnappers crystals that show the same pattern of zonation. The corresponding population of Rocky Hill orthopyroxenes can thus be considered as remnants from the final melt dominant bodies which were made more eruptible prior to, but not fully evacuated during, the Kidnappers event. Consistent with this inference, the majority of modelled ages from the dark exterior zone in Rocky Hill orthopyroxenes, including those from the dark zone to outermost rim boundary, are greater than those from the Kidnappers. The offset in the peak PDF value of ages derived for this common zonation (~10 years) therefore represents one indirect estimate of the time break between the two eruptions (Figs. 4, 7). All crystals that returned modelled ages of >10 years are therefore inferred to be inherited from Kidnappers magma/mush. The textures and chemical zoning within the majority of Rocky Hill orthopyroxenes (and other mineral phases) do not contain any evidence for a priming or trigger mechanism for the eruption analogous to that seen in the Kidnappers KI-3 pumice group.

6.2. Implications of diffusion timescales from orthopyroxene core-rim boundaries

Prominent core-rim boundaries within orthopyroxenes from the Kidnappers/Rocky Hill samples are inferred to represent a transition from storage in a crystal mush to holding and further crystallization within the melt-dominant bodies that were finally erupted (Cooper et al., 2016). Timescales modelled across Kidnappers core-rim boundaries cover a large range, but only one crystal returns an age of >600 years before eruption. 72 % of diffusion profiles date to within 200 years of the eruption and suggests that a significant input of orthopyroxene grains (those displaying normal zonation: Supplementary Fig. 2) to the final melt-dominant body occurred within centuries (Fig. 8) and that this process peaked only

decades prior to the Kidnappers eruption (Fig. 4). The Fe-Mg modelled diffusion ages across Kidnappers/Rocky Hill orthopyroxene core-rim boundaries cover similar timescales to those inferred from those corresponding crystal boundaries recorded in the Oruanui (Allan et al., 2013), which are also inferred to represent the timing of physical extraction and establishment of the melt-dominant body. In the Oruanui case, ~90 % of orthopyroxenes record this common history (Allan et al., 2013), but within the Kidnappers the proportion of crystals recording this process is lower and varies between compositional groups (34-76 %) (Table 2), suggesting that additional controls were operating within the Mangakino magmatic system. The proportion of nominally unzoned grains within the Kidnappers ranges between 15 and 51 %. These crystals either entirely grew within a melt-dominant body prior to eruption or were introduced into the melt-dominant bodies sufficiently close to the time of eruption so as not to be able to grow a discernible contrasting rim.

Core-rim boundaries within Rocky Hill orthopyroxenes record a similar range of timescales as in Kidnappers grains. The Rocky Hill core-rim model ages, which reflect the timing of movement of orthopyroxene grains to the final erupted melt-dominant body, have a peak PDF age at ~40 years (Fig. 4). This ~40 year peak is inferred to correspond to the same peak input of grains ~20 years prior to the Kidnappers eruption. There is a continuity of core-rim ages within this ~20 year window, suggesting that there was a sustained movement of crystals from the mush zone to melt dominant bodies during the time break between the two eruptions (Fig. 8). This feature is particularly marked in orthopyroxenes from the high-SiO₂ Rocky Hill (RH-2) pumice group, where 94 % of grains have normal zonation. This dominant zonation pattern is coupled with lower amphibole rim model temperature and pressure estimates, low-An plagioclase rims, and lower-Ca homogeneous glass (Cooper et al., 2016). These distinctive characteristics of the RH-2 pumice group support the idea that a significant proportion of magma was newly assembled into eruptible melt dominant bodies, with most of

the incorporated orthopyroxenes recording a post-Kidnappers magmatic history. Grains which return core-rim model ages greater than a few hundred years are likely inherited from the earlier Kidnappers system, and record common precursor processes within the common magma system.

Differences in the model timescales from the core-rim boundaries between both eruptions are consistent with the field evidence for a short time break between these eruptions. Although the resolution of the data is lower than ages from the dark outer zones, there is a ~20 year difference in core-rim model age peaks between the two eruptions, which is the same, within uncertainties, as the independently estimated ~10 year time break observed across dark outer zones. It is not possible to definitively estimate the time break between the Kidnappers and Rocky Hill eruptions with diffusion timescales alone, due to their inherent imprecision. Two further, independent lines of field evidence support such a short time gap. (1) The erosional contact between the two ignimbrites has no associated development of a soil horizon (Cooper et al., 2016). (2) The associated fall and reworked material (collectively referred to as the Potaka Tephra: Shane, 1994; Carter et al., 2004), both on land and in marine cores compositionally appears to be a single composite deposit of primary and reworked Kidnappers and Rocky Hill material (Cooper et al., 2012).

6.3. Consequences of short quartz diffusion timescales

The similarity of Ti in quartz timescales and orthopyroxene Fe-Mg interdiffusion timescales (Fig. 7) suggests that they are recording the same, or concurrent, processes within the Kidnappers and Rocky Hill magmatic system prior to the eruption of the former. It is remarkable that even intermediate domains within quartz return timescales within 30 years of eruption. This supports the idea of rapid crystallization of quartz prior to eruption (Gualda and Sutton, 2016), but is not consistent with the notion that the CL-brighter rims on the quartz

crystals are the result of syn-eruptive rapid growth associated with magma ascent (cf. Pamukcu et al., 2016). Commonly, Kidnappers and Rocky Hill quartz grains record multiple resorption episodes, suggesting that quartz can cycle many times between dissolution and growth over geologically short timescales. Therefore we infer that the majority of quartz timescales likely record only the latest episodes of crystal growth within the erupted magma (at temperatures below the incoming of quartz in the crystallising assemblage and above the solidus) prior to eruption. Quartz grains may have been stored in a mush over a much longer timescale than is recorded by Ti-in-quartz diffusion prior to remobilization and dissolution followed by rapid regrowth (Cooper and Kent, 2014).

6.4. Timescale comparisons and considerations

Values chosen for the parameters (particularly temperature) used in Fe-Mg diffusion modelling calculations have a large influence on the modelled ages. All age estimates reported here are maxima and the timescales discussed above are upper-bound limits, based on an assumed initial sharp profile. In Rocky Hill orthopyroxenes, analogous zones were modelled at conditions that reflected the outer rim growth of crystals and not necessarily the original conditions under which the dark zone formed (Table 1). Therefore, we need to rule out the possibility of using lower temperature estimates (765-795 °C) to artificially produce larger age estimates in Rocky Hill orthopyroxenes. If 820 °C was used in calculations of Rocky Hill darker exterior zone ages, the range of modelled ages would be reduced from 10-238 to 5-128 years. All modelled Rocky Hill ages (peak PDF at ~7 years) would still be older than the <3 yr peak within the Kidnappers, therefore halving the estimated time-break between eruptions. Therefore the disparities in ages calculated using different temperature estimates are not large enough to substantively change any of our conclusions.

Timescales from Fe-Ti interdiffusion within orthopyroxene and Ti-in quartz diffusion

calculated using the methods described above are comparable with one another (Fig. 7). This is in contrast to crystals from the Bishop Tuff (Chamberlain et al., 2014), in which orthopyroxene timescales were an order of magnitude shorter than those from quartz. This difference between our results and those of Chamberlain et al. (2014) may be a consequence of us removing the oxygen fugacity correction from the Fe-Mg interdiffusion equation, which shifts timescales 0.75 log units towards longer timescales. There is a wide range of published orthopyroxene partition coefficients (Ganguly and Tazzoli, 1994; Schwandt et al., 1998; Dohmen et al., 2016), use of which result in correspondingly diverse timescales. The similarity of the timescales determined for different mineral species in this study give us confidence that the Fe-Mg interdiffusion coefficient used here is suitable for the orthopyroxene compositions and conditions relevant for the Mangakino magmatic system.

The timescales obtained from orthopyroxenes and quartz are much shorter than the inferred lifetime of the Kidnappers/Rocky Hill system from zircon U-Pb age spectra (Cooper et al., 2014). The zircon age spectra suggest that the common system was developed over a ~200 kyr period, with a peak crystallization age mode within uncertainty of the eruption age at 1.0 Ma. The age contrasts are a consequence of the processes being recorded by each technique. U-Pb zircon age spectra provide a ~200 kyr record for the overall assembly of the magma system, specifically the time when zircon began crystallizing within the system. In contrast, the orthopyroxene Fe-Mg interdiffusion and Ti in quartz diffusion timescales record assembly of the final melt-dominant bodies and processes of recharge within the magma system. The melt-dominant bodies were largely established <600 years before eruption, with a significant input of material within centuries to decades of each eruption. The timescales we present support the idea that magma in large silicic systems may only have a short time window where it is in a melt-rich state during which it can erupt (e.g. Allan et al., 2013; Cooper and Kent, 2014; Barker et al., 2016).

Timescales for the assembly of the Kidnappers/Rocky Hill system, as well as the establishment of melt-dominant bodies are similar to contrasting timescales recorded in the ~350 ka Whakamaru ignimbrite, New Zealand. Here zircon U-Pb age spectra indicate magmatic residence times of 250 kyr prior to eruption, with periods of crystallization closer to eruption following magmatic events (Brown and Fletcher, 1999). Saunders et al. (2010) and Matthews et al. (2012a, b) investigated the timescales of quartz crystallization in the Whakamaru deposits on the basis of Ti diffusion in quartz. They found that a significant chemical change occurred in the Whakamaru system <300 yrs before eruption and peaked at ~10-85 years. This change is interpreted to represent a rapid thermal pulse or pressure change accompanying late-stage magma chamber recharge. Like the dark exterior zones within orthopyroxene and up-temperature plagioclase and amphibole rims in the KI-3 compositional group seen in the Kidnappers deposits, this late-stage Whakamaru quartz signal was attributed by Matthews et al. (2012a, b) to open-system processes and the rejuvenation of rhyolitic magma by interaction with underplated mafic magma. Comparable rejuvenation timescales are also proposed in the ~61 ka Earthquake Flat eruption, Okataina, New Zealand and the ~74 ka Youngest Toba Tuff supereruption, Sumatra (Matthews et. al., 2012a; Budd et al., 2017). Similarly short timescales for the physical remobilisation of felsic magmas are being reported for eruptions of a range of scales at many other volcanoes worldwide for historic and prehistoric eruptions, e.g. Vesuvius (Morgan et al., 2004, 2006), Santorini (Druitt et al., 2012) and Huaynaputina (de Silva et al., 2008)

The acceleration of the magmatic system towards eruption implied by the Kidnappers and Rocky Hill orthopyroxene and quartz timescales suggest that dynamic, open-system processes occurred shortly before eruption and raises questions as to what the trigger mechanism for each eruption was. It is hard to envisage how an exceptionally large silicic system could erupt ~1200 km³ of material, before shutting down for 1-2 decades before the

evacuation of another $\sim 200 \text{ km}^3$ of material without an external control. There is growing evidence for a strong tectonic control on magmatic systems within the TVZ (e.g. Rowland et al., 2010; Allan et al., 2012) and we suggest that rifting-related tectonic processes may have exerted a dominant control on both the triggering and intervening shutdown of the Kidnappers and Rocky Hill eruptions.

7. Conclusions

Orthopyroxene and quartz from the Kidnappers and Rocky Hill contain textural and chemical features that record open-system processes shortly before each eruption. Diffusion modelling of textural zones within both mineral phases are concordant and suggest timescales within centuries to years of the following processes.

(1) Movement of crystals and melt from a large-volume crystal mush to assemble the final melt-dominant bodies occurred within centuries of the Kidnappers eruption. This process was most prevalent only ~ 20 years prior to eruption.

(2) Interaction of a less-evolved melt with some part of the Kidnappers magma system occurred within 30 years of eruption and was most prevalent in the decade prior to eruption. This interaction, possibly through mafic underplating, remobilized a volume of crystal mush which contributed crystals and melt towards the generation of the KI-3 eruptible magma just prior to eruption.

(3) Difference in Fe-Mg interdiffusion model ages from dark exterior zones and core-rim boundaries between samples from the Kidnappers and Rocky Hill deposits yield estimates of the time break between the eruptions of one or two decades. This short time break, represented by an erosion surface in the field, highlights the rapidity of magmatic rejuvenation at Mangakino following the Kidnappers supereruption.

(4) The rapidity of quartz crystallization shown by diffusive modelling of internal zone

boundaries suggests that quartz is a transient phase in the Kidnappers/Rocky Hill magmatic system. Quartz is always present, but textural evidence indicates individual crystals are undergoing multiple resorption episodes, often to complete dissolution, followed by growth of new zones or complete crystals. Diffusion timescales in quartz are thus only reflecting the latest episodes of crystal growth prior to eruption, at temperatures below the incoming of quartz in the crystallising assemblage and above the solidus.

Acknowledgements

Richard Walshaw is thanked for assistance with CL imaging at the University of Leeds. Katy Chamberlain, Aidan Allan and Simon Barker are thanked for valuable discussions during the preparation of this manuscript. We thank Victoria University for a PhD Scholarship for GFC, and the Royal Society of New Zealand for support from the Marsden Fund (VUW0813) and for a James Cook Fellowship for CJNW. Participation of DJM was made possible through the Marsden Fund grant VUW0813. We thank Georg Zellmer and an anonymous reviewer for constructive comments on the submitted manuscript and Tamsin Mather for editorial handling.

References

- Allan, A.S.R., Wilson, C.J.N., Millet, M-A., Wysoczanski, R.J., 2012. The invisible hand: tectonic triggering and modulation of a rhyolitic supereruption. *Geology* 40, 563–566.
- Allan, A.S.R., Morgan, D.J., Wilson, C.J.N., Millet, M-A., 2013. From mush to eruption in centuries: assembly of the super-sized Oruanui magma body. *Contributions to Mineralogy and Petrology* 166, 143–164.
- Bachmann, O., Bergantz, G.W., 2004. On the origin of crystal-poor rhyolites: extracted from batholithic crystal mushes. *Journal of Petrology* 45, 1565–1582.

597 Barker, S.J., Wilson, C.J.N., Morgan, D.J., Rowland, J.V., 2016. Rapid priming,
 598 accumulation and recharge of magma driving recent eruptions at a hyperactive caldera
 599 volcano. *Geology* 44, 323–326.

600 Besancon, J.R., 1981. Rate of cation ordering in orthopyroxenes. *American Mineralogist* 66,
 601 965–973.

602 Blundy, J., Cashman, K., 2008. Petrologic reconstruction of magmatic system variables and
 603 processes. *Reviews in Mineralogy and Geochemistry* 69, 179-239.

604 Brown, S.J.A., Fletcher, I.R., 1999. SHRIMP U-Th dating of the preeruption growth history
 605 of zircons from the 340 ka Whakamaru Ignimbrite, New Zealand: evidence for >250 k.y.
 606 magma residence times. *Geology* 27, 1035–1038.

607 Budd, D.A., Troll, V.R., Deegan, F.M., Jolis, E.M., Smith, V.C., Whitehouse, M.J., Harris, C., Freda,
 608 C., Hilton, D.R., Halldórsson, S.A., Bindeman, I.N. 2017. Magma reservoir dynamics at Toba
 609 caldera, Indonesia, recorded by oxygen isotope zoning in quartz. *Scientific Reports* 7, 40624.

610 Carter, L., Alloway, B.V., Shane, P., Westgate, J.A., 2004. Deep-ocean record of major late Cenozoic
 611 rhyolitic eruptions from New Zealand. *New Zealand Journal of Geology and Geophysics* 47,
 612 481–500.

613 Chakraborty, S., 2008. Diffusion in solid silicates: a tool to track timescales of processes
 614 comes of age. *Annual Review of Earth and Planetary Sciences* 36, 153–190.

615 Chamberlain, K.J., Morgan, D.J., Wilson, C.J.N., 2014. Timescales of mixing and
 616 mobilisation in the Bishop Tuff magma body: perspectives from diffusion chronometry.
 617 *Contributions to Mineralogy and Petrology* 168, Art. No. 1034.

618 Cherniak, D.J., Watson, E.B., Wark, D.A., 2007. Ti diffusion in quartz. *Chemical Geology*
 619 236, 65-74.

620 Cooper, G.F., Wilson, C.J.N., Millet, M-A., Baker, J.A., Smith, E.G.C., 2012. Systematic
621 tapping of independent magma chambers during the 1 Ma Kidnappers supereruption.
622 Earth and Planetary Science Letters 213-214, 23–33.

623 Cooper, G.F., Wilson, C.J.N., Charlier, B.L.A., Wooden, J.L., Ireland, T.R., 2014. Temporal
624 evolution and compositional signatures of two supervolcanic systems recorded in
625 zircons from Mangakino Volcanic Centre, New Zealand. Contributions to Mineralogy
626 and Petrology 167, 1018.

627 Cooper, G.F., Wilson, C.J.N., Millet, M-A., Baker, J.A., 2016. Generation and rejuvenation of
628 a supervolcanic magmatic system: a case study from Mangakino volcanic centre, New
629 Zealand. Journal of Petrology 57, 1135–1170.

630 Cooper, K.M., Kent, A.J., 2014. Rapid remobilization of magmatic crystals kept in cold
631 storage. Nature 506, 480–483.

632 Costa, F., Morgan, D., 2010. Time constraints from chemical equilibration in magmatic
633 crystals. In: Dosseto, A., Turner, S.P., Van Orman, J.A. (Eds.), Timescales of magmatic
634 processes: from core to atmosphere. Wiley, Chichester, UK, p. 129–159.

635 Costa, F., Dohmen, R. and Chakraborty, S., 2008. Time scales of magmatic processes from
636 modeling the zoning patterns of crystals. Reviews in Mineralogy and Geochemistry 69,
637 545-594. Crank, J., 1979. The Mathematics of Diffusion. Oxford University Press,
638 Oxford, UK.

639 Davies, G.R., Halliday, A.N., Mahood, G.A., Hall, C.M., 1994. Isotopic constraints on the
640 production rates, crystallization histories and residence times of pre-caldera silicic
641 magmas, Long Valley, California. Earth and Planetary Science Letters 125, 17-37.

642 de Silva, S., Salas, G., Schubring, S., 2008. Triggering explosive eruptions: the case for
643 silicic magma recharge at Huaynaputina, southern Peru. Geology 36, 387–390.

644 Dohmen, R., Chakraborty, S., 2007. Fe-Mg diffusion in olivine II: point defect chemistry,
645 change in diffusion mechanisms and a model for calculation of diffusion coefficients
646 in natural olivine. *Physics and Chemistry of Minerals* 34, 409-430.

647 Dohmen, R., Ter Heege, J.H., Becker, H.-W., Chakraborty, S., 2016. Fe-Mg interdiffusion in
648 orthopyroxene. *American Mineralogist* 101, 2210-2221.

649 Druitt, T.H., Costa, F., Deloule, E., Dungan, M.A., Scaillet, B., 2012. Decadal to monthly
650 timescales of magma transfer and reservoir growth at a caldera volcano. *Nature* 482,
651 77–80.

652 Ganguly, J., Tazzoli, V., 1994. Fe²⁺-Mg interdiffusion in orthopyroxene: retrieval from the
653 data on intracrystalline exchange reaction. *American Mineralogist* 79, 930–937.

654 Gualda, G.A.R., Sutton, S.R., 2016. The year leading to a supereruption. *PLoS One* 11:
655 e0159200.

656 Gualda, G.A.R., Pamukcu, A.S., Ghiorso, M.S., Anderson, A.T., Sutton, S.R., Rivers, M.L.,
657 2012. Timescales of quartz crystallization and the longevity of the Bishop giant magma
658 body. *PLoS ONE*, 7, e37492.

659 Hildreth, W., 2004. Volcanological perspectives on Long Valley, Mammoth Mountain, and
660 Mono Craters: several contiguous but discrete systems. *Journal of Volcanology and*
661 *Geothermal Research* 136, 169–198.

662 Kahl, M., Chakraborty, S., Costa, F., Pompilio, M., Liuzzo, M., Viccaro, M., 2013.
663 Compositionally zoned crystals and real-time degassing data reveal changes in magma
664 transfer dynamics during the 2006 summit eruptive episodes of Mt. Etna. *Bulletin of*
665 *Volcanology* 75, 692.

666 Martin, V.M., Morgan, D.J., Jerram, D.A., Caddick, M.J., Prior, D.J., Davidson, J.P., 2008.
667 Bang! Month-scale eruption triggering at Santorini Volcano. *Science* 321, 1178.

668 Matthews, N.E., Huber, C., Pyle, D.M., Smith, V.C., 2012a. Timescales of magma recharge
 669 and reactivation of large silicic systems from Ti diffusion in quartz. *Journal of*
 670 *Petrology* 53, 1385–1416.

671 Matthews, N.E., Pyle, D.M., Smith, V.C., Wilson, C.J.N., Huber, C., van Hinsberg, V., 2012b.
 672 Quartz zoning and the pre-eruptive evolution of the ~340-ka Whakamaru magma
 673 systems, New Zealand. *Contributions to Mineralogy and Petrology* 163, 87–107.

674 Morgan, D.J., Blake, S., Rogers, N.W.B., DeVivo, B., Rolandi, G., Macdonald, R.,
 675 Hawkesworth, C.J., 2004. Time scales of crystal residence and magma chamber volume
 676 from modelling of diffusion profiles in phenocrysts: Vesuvius 1944. *Earth and*
 677 *Planetary Science Letters* 222, 933–946.

678 Morgan, D.J., Rogers, N.W., Blake, S., De Vivo, B., Rolandi, G., Davidson, J.P., 2006.
 679 Magma recharge at Vesuvius in the century prior to AD79. *Geology* 34, 845-848.

680 Pamukcu, A.S., Ghiorso, M.S., Gualda, G.A.R., 2016. High-Ti, bright-CL rims in volcanic
 681 quartz: a result of very rapid growth. *Contributions to Mineralogy and Petrology* 171,
 682 105.

683 Ridolfi, F., Renzulli, A., Puerini, M., 2010. Stability and chemical equilibrium of amphibole
 684 in calc-alkaline magmas: an overview, new thermobarometric formulations and
 685 application to subduction-related volcanoes. *Contributions to Mineralogy and Petrology*
 686 160, 45-66.

687 Rowland, J.V., Wilson, C.J.N., Gravley, D.M., 2010. Spatial and temporal variations in
 688 magma-assisted rifting, Taupo Volcanic Zone, New Zealand. *Journal of Volcanology*
 689 *and Geothermal Research* 190, 89–108.

690 Saunders, K.E., Morgan, D.J., Baker, J.A., Wysoczanski, R.J., 2010. The magmatic evolution
 691 of the Whakamaru supereruption, New Zealand, constrained by a microanalytical study
 692 of plagioclase and quartz. *Journal of Petrology* 51, 2465-2488.

693 Saunders, K., Blundy, J., Dohmen, R., Cashman, K., 2012. Linking petrology and seismology
 694 at an active volcano. *Science* 336, 1023–1027.

695 Sautter, V., Jaoul, O., Abel, F., 1988. Aluminum diffusion in diopside using the $^{27}\text{Al}(p,\gamma)^{28}\text{Si}$
 696 nuclear reaction: preliminary results. *Earth and Planetary Science Letters* 89, 109–114.

697 Schmitt, A.K., 2011. Uranium series accessory crystal dating of magmatic processes. *Annual*
 698 *Review of Earth and Planetary Sciences* 39, 321–349.

699 Schwandt, C.S., Cygan, R.T., Westrich, H.R., 1998. Magnesium self-diffusion in orthenstatite.
 700 *Contributions to Mineralogy and Petrology* 130, 390–396.

701 Shane, P.A.R., 1994. A widespread, early Pleistocene tephra (Potaka tephra, 1 Ma) in New
 702 Zealand: character, distribution, and implications. *New Zealand Journal of Geology and*
 703 *Geophysics* 37, 25–35.

704 Smith, D., Barron, B.R., 1991. Pyroxene-garnet equilibration during cooling in the mantle.
 705 *American Mineralogist* 76, 1950–1963.

706 Turner, S., Costa, F., 2007. Measuring timescales of magmatic evolution. *Elements* 3, 267-
 707 272.

708 Wark, D.A., Hildreth, W., Spear, F.S., Cherniak, D.J., Watson, E.B., 2007. Pre-eruption
 709 recharge of the Bishop magma system. *Geology* 35, 235–238.

710 Wilson, C.J.N., Charlier, B.L.A., 2009. Rapid rates of magma generation at contemporaneous
 711 magma systems, Taupo volcano, New Zealand: insights from U-Th model-age spectra
 712 in zircons. *Journal of Petrology* 50, 875–907.

713 Wilson, C.J.N., Houghton, B.F., Kamp, P.J.J., McWilliams, M.O., 1995. An exceptionally
 714 widespread ignimbrite with implications for pyroclastic flow emplacement. *Nature* 378,
 715 605–607.

716 Wilson, C.J.N., Gravley, D.M., Leonard, G.S., Rowland, J.V., 2009. Volcanism in the central
 717 Taupo Volcanic Zone, New Zealand: tempo, styles and controls. In: Thordarson, T.,

718 Self, S., Larsen, G., Rowland, S.K., Hoskuldsson, A. (Eds), Studies in Volcanology:
719 The Legacy of George Walker. Special Publications of IAVCEI 2, 225-247.
720
721

Figure captions

Fig. 1. Map of the North Island, New Zealand showing the location of the Mangakino caldera and extent of the Kidnappers and Rocky Hill ignimbrites. Sample site locations used in this study are shown. Modified from Cooper et al. (2016).

Fig. 2. Back-scattered electron (BSE) images and associated profiles to assess the effect of uncertainties due to image resolution and associated convolution. (a) image at x120 magnification and imaged at faster scan speeds ('Fine 1') which imparts a larger pixel size on the area of the profile. (b) image at x370 magnification and slower scan speeds ('Fine 2') resulting in smaller pixels. The effect of flaring across a demonstrably sharp stepwise boundary (i.e. the edge of the crystal) is also shown.

Fig. 3. Selected examples of orthopyroxene BSE images of crystals extracted from pumices within the Kidnappers (group KI-3) and Rocky Hill (groups RH-1 and RH-2) deposits with corresponding modelled Fe-Mg diffusion profiles taken across boundaries (yellow box areas). Profiles of greyscale intensity are taken from rotated BSE images, and are converted to Mg #. The red line shows each modelled profile of an initially sharp compositional boundary over the time presented for each profile, using the parameters in Table 1.

Fig. 4. Histograms showing the range and frequency of maximum Fe-Mg interdiffusion ages determined in orthopyroxene crystals for the core-rim boundaries from the Kidnappers (a) and Rocky Hill (b), and from dark exterior zones in the Kidnappers (c) and Rocky Hill (d). The PDF curve (Kidnappers in red, Rocky Hill in green) represents a population probability of all age determinations with associated uncertainties resulting from the precision of temperature estimates (± 30 °C).

Fig. 5. (a) An example of a quartz cathodoluminescence (CL) image from the Kidnappers (sample P2006 from KI-2) with corresponding modelled Ti-in-quartz diffusion profiles from two selected CL-defined boundaries (b & c).

Fig. 6. Histograms showing the range and frequency of maximum Ti in quartz ages determined for all quartz boundaries from the Kidnappers (a) and Rocky Hill (b).

Fig. 7. Summary stacked plots of the model ages derived from diffusion profiles in all samples analysed. (a) Orthopyroxene Fe-Mg interdiffusion ages and their absolute uncertainties (coloured bands: red – Kidnappers; yellow = Rocky Hill) from dark outer zones in the crystals. Note the distinct contrast between the values from the two deposits, interpreted to reflect the time gap between the two eruptions. (b) Fe-Mg interdiffusion ages and their absolute uncertainties from orthopyroxene core-rim boundaries. (c) Ti-in-quartz ages and uncertainties.

Fig. 8. Cartoon cross section of the Kidnappers/Rocky Hill magma system at two stages: (1) prior to eruption of the Kidnappers and (2) during the short time break between eruptions. The magmatic processes inferred from crystal textures and chemistry (discussed in the text), over the timescales modelled from Fe-Mg interdiffusion in orthopyroxene are shown.

Table 1. Summary of orthopyroxene textural populations.

Groups and samples	Temperature	fO_2 (ΔNNO)	Normal	Reverse	Unzoned	Patchy	Dark outer
Kidnappers							
KI-3 (low-SiO₂)	820 °C	0.1	34.0 %	7.6 %	51.4 %	6.9 %	41.0 %
P1655, P17XX							

KI-1 (mid-SiO₂)	785 °C	0.0	53.1 %	3.1 %	42.2 %	1.6 %	5.5 %
-----------------------------------	--------	-----	--------	-------	--------	-------	-------

P1646, P1649,
P2011

KI-2 (high-SiO₂)	780 °C	0.2	76.2 %	1.2 %	15.2 %	7.3 %	2.4 %
------------------------------------	--------	-----	--------	-------	--------	-------	-------

P1607, P1609,
P2006, P2015

Rocky Hill

RH-1 (normal)	795 °C	0.1	54.7 %	6.6 %	38.1 %	0.6 %	13.2 %
----------------------	--------	-----	--------	-------	--------	-------	--------

P2000, P2029,
P2042, P2049,
P2050

RH-2 (high SiO₂)	765 °C	0.0	94.3 %	1.1 %	4.6 %	0.0 %	1.1 %
------------------------------------	--------	-----	--------	-------	-------	-------	-------

P2046

Temperatures presented were used to calculate orthopyroxene diffusive timescales from each compositional group from the Kidnappers and Rocky Hill.

Table 2. Summary of quartz textural populations.

Groups and samples	Temperature	Dark rim	Light rim	No significant change
Kidnappers				
KI-2 (P2006)	780 °C	80 %	7 %	13 %
Rocky Hill				
RH-1 (P2050)	795 °C	19.5 %	61 %	19.5 %

Textural classification is based on CL intensities. Temperatures presented were used to calculate quartz diffusive timescales.

Supplementary figure captions

Fig. S1. Plot to demonstrate the strong correlation between greyscale intensity and the Mg-Fe proportions of orthopyroxenes analysed for this study. The correlation was measured over 24 crystals, imaged under identical settings and analysed within a single analytical session on a JEOL JXA-8230 electron microprobe at Victoria University of Wellington.

Fig. S2. Summary of textural features (based on BSE imaging) of Kidnappers and Rocky Hill orthopyroxene grains in each pumice compositional group. The dark exterior zone may be superimposed on any of the four other textures. Diagram modified from Cooper et al. (2016).

Fig. S3. Element maps of a representative normally zoned orthopyroxene crystal with a dark core from the Rocky Hill (pumice P2046 from compositional group RH-2 [Cooper et al., 2016]). The Al map shows blurring of the core-rim boundary parallel to the *c*-axis compared to along the *a*-axis, suggesting a strong growth control parallel to the *c*-axis. Slowly diffusing Ca shows dissolution of the core, and formation of melt inclusions during recrystallization. Ca-poor haloes around melt inclusions within the orthopyroxene represent secondary zonation caused by dissolution and formation of Ca-rich melt inclusions, before crystallization resumed. Melt inclusions in the core thus record a departure from equilibrium for a period of time and dissolution of the crystal before growth was resumed and the crystal rim formed within the final erupted melt dominant bodies. The Mg + Fe map highlights streaky zones, which are often, but not always, visibly associated with inclusions and may represent the result of diffusion from an inclusion above or beneath the plane of the polished surface, or a recrystallization trail from a mobile melt inclusion.

Fig. S4. Element maps of a representative orthopyroxene crystal from the Rocky Hill (pumice P2049 from compositional RH-1) with a dark exterior zone. Elements with very slow (Al) and slow (Ca) diffusion rates preserve the original zonation to a greater extent than faster diffusing Mg. The map of Mg content and BSE image show increased blurring of the dark zone, parallel to the *c*-axis, compared to across the *a*-axis, inferred to reflect a component of growth zonation along the *c*-axis.

Figure 1
[Click here to download Figure: Fig. 1.pdf](#)

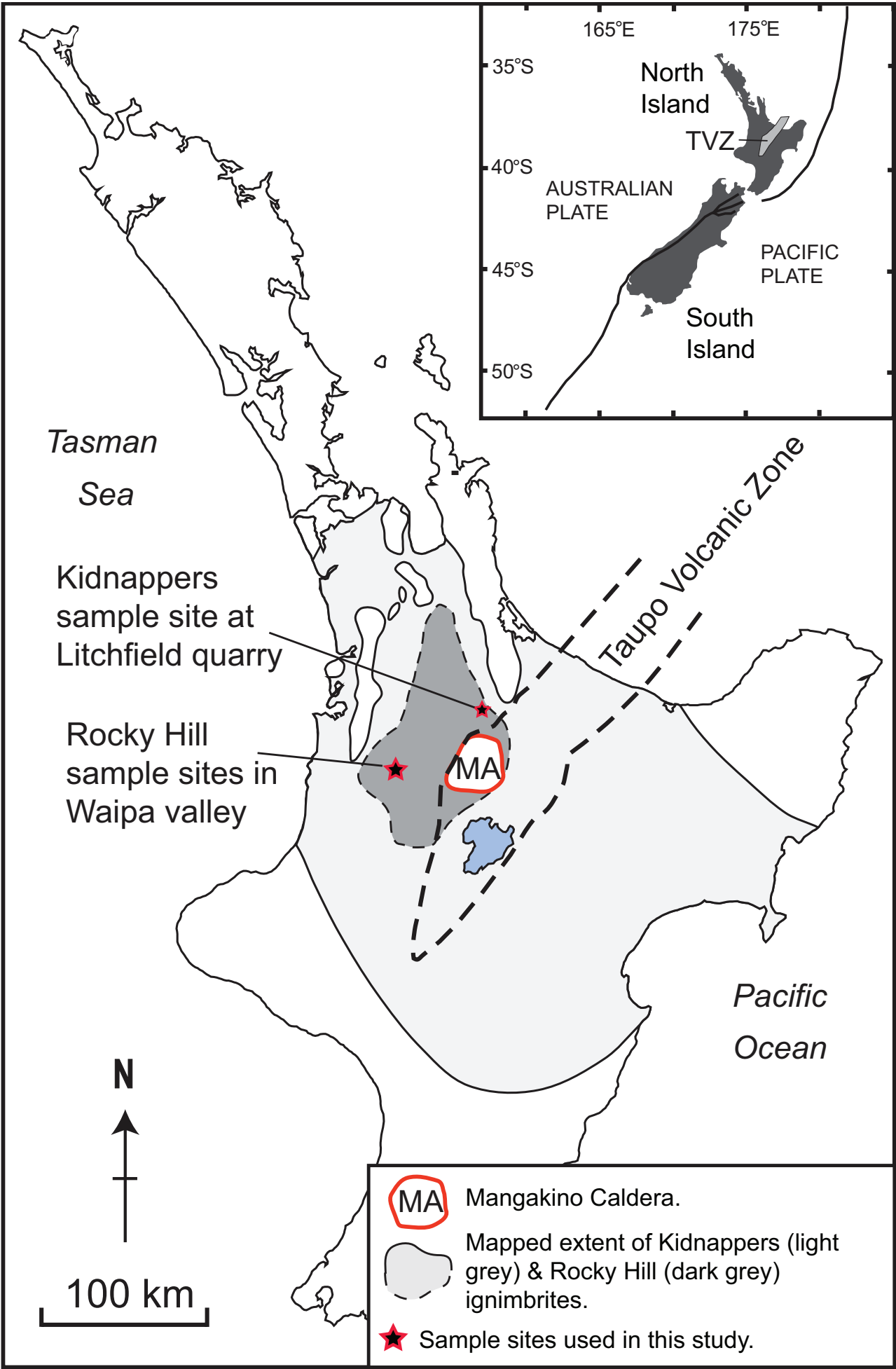
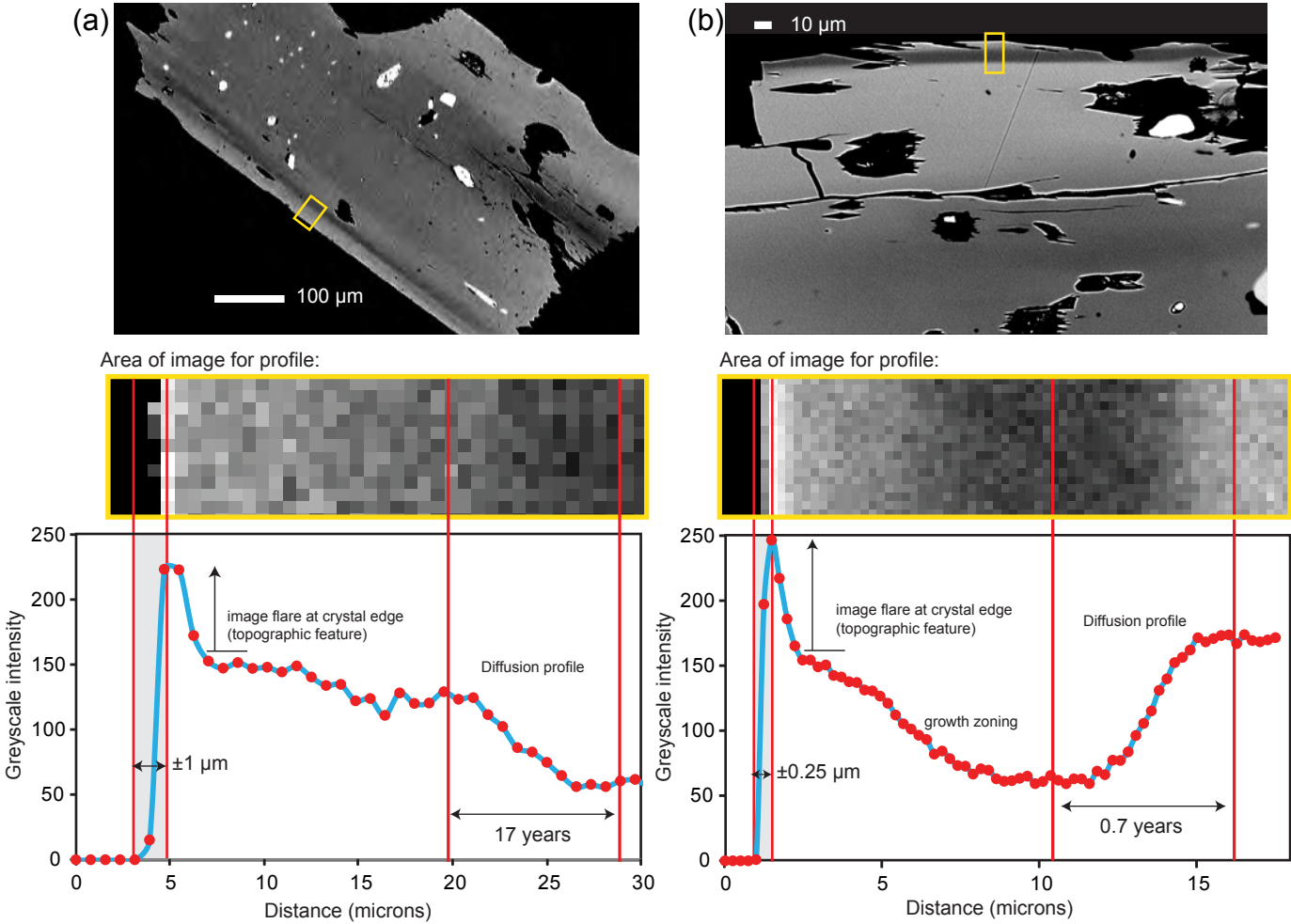
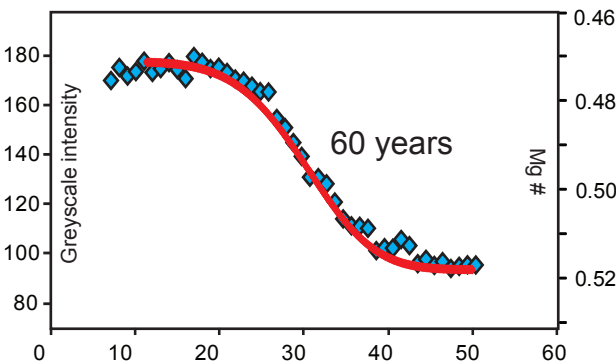
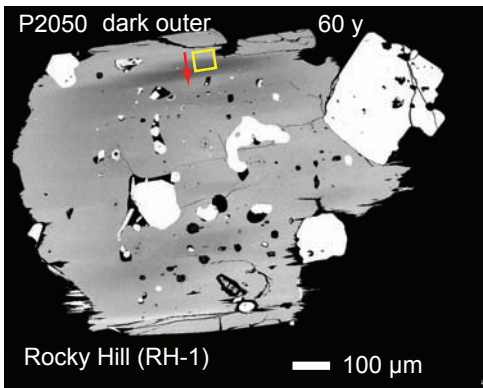
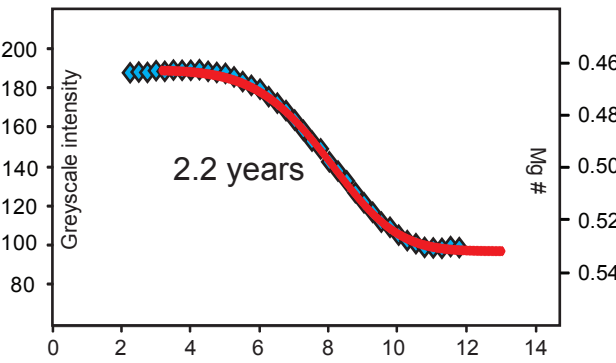
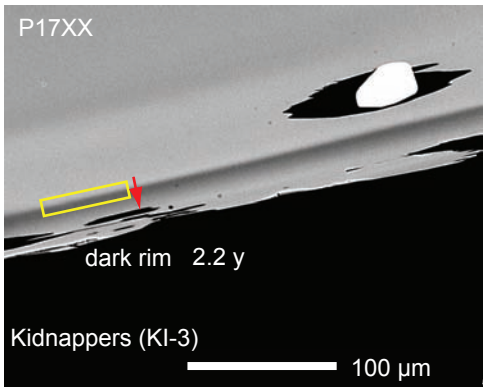
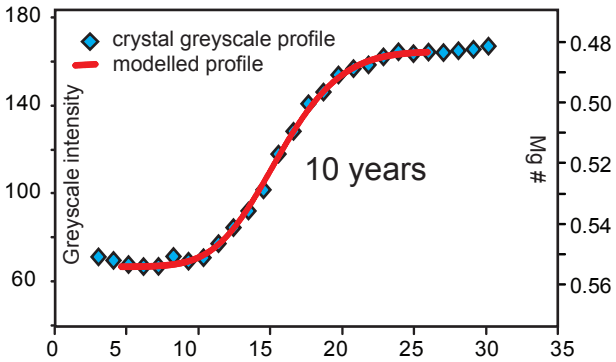
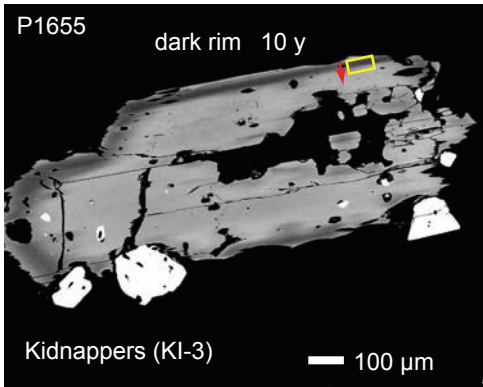


Figure 2
Click here to download Figure: Fig. 2.pdf



Dark exterior zones



Core-rim boundary

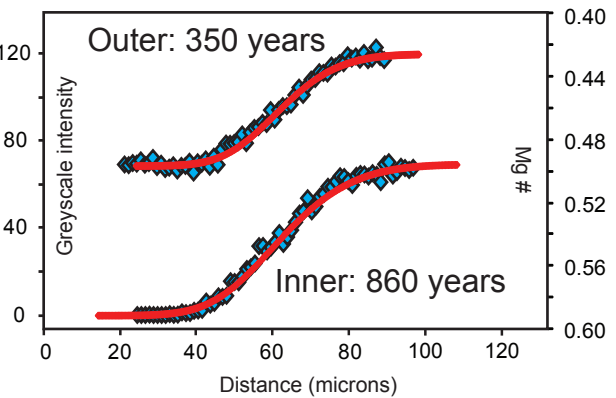
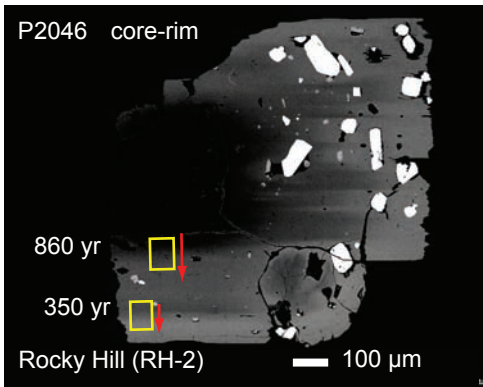
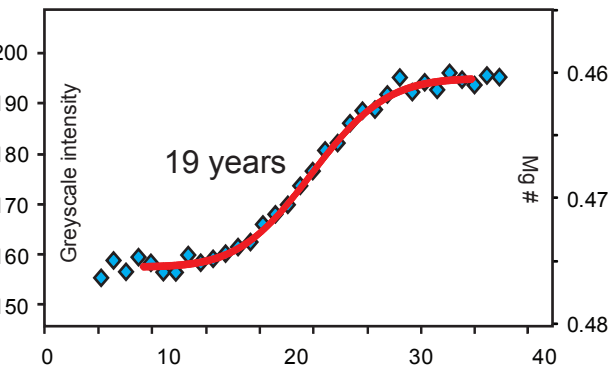
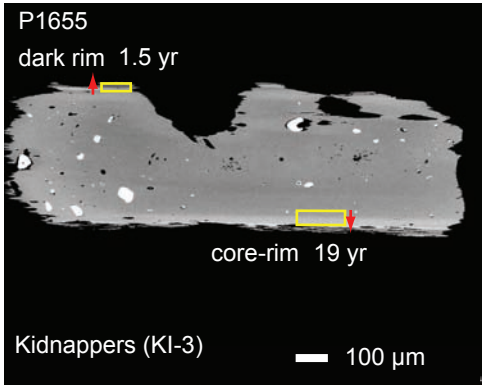


Figure 4
[Click here to download Figure: Fig. 4.pdf](#)
Fig. 4

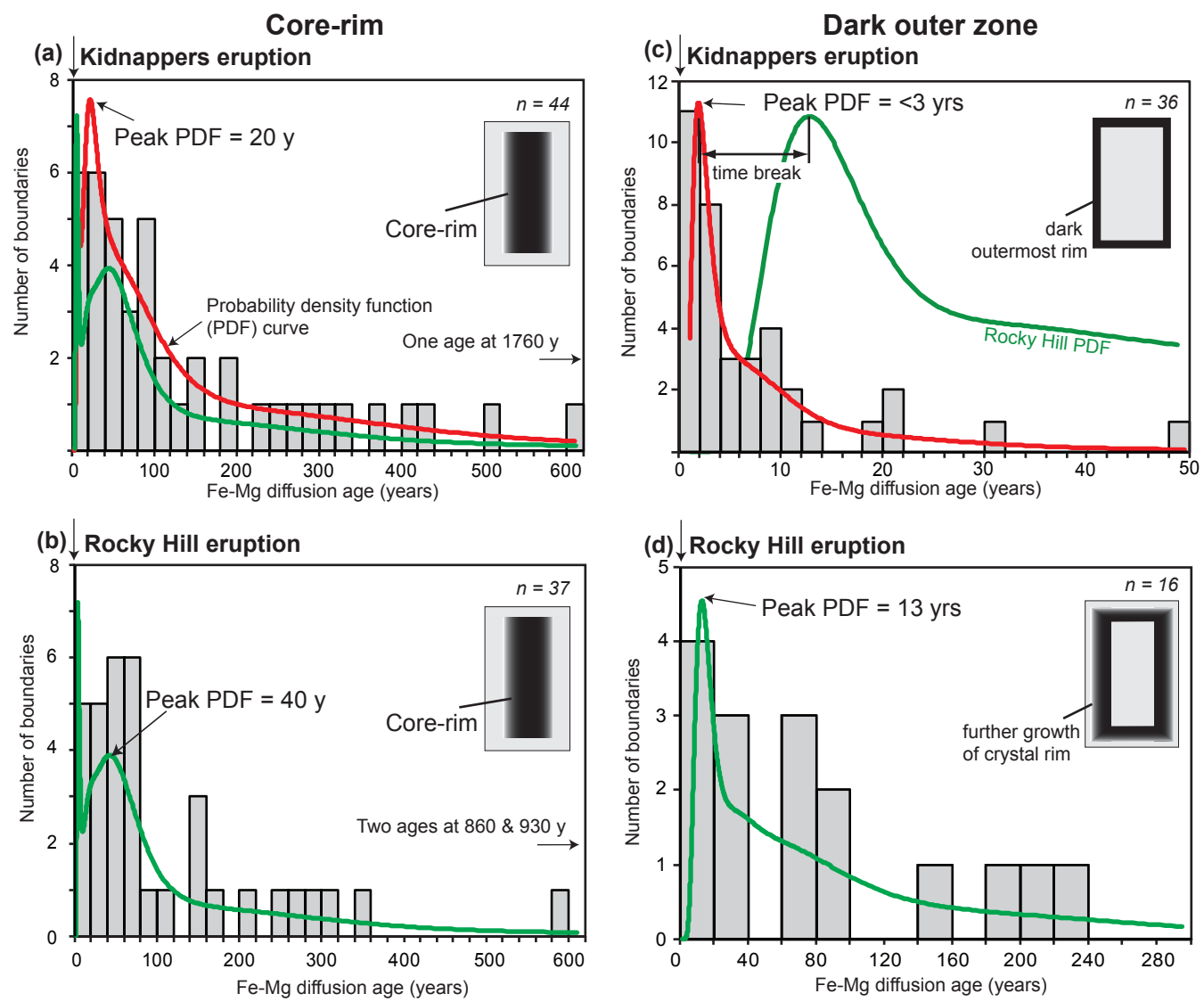


Figure 5
[Click here to download Figure: Fig. 5.pdf](#)

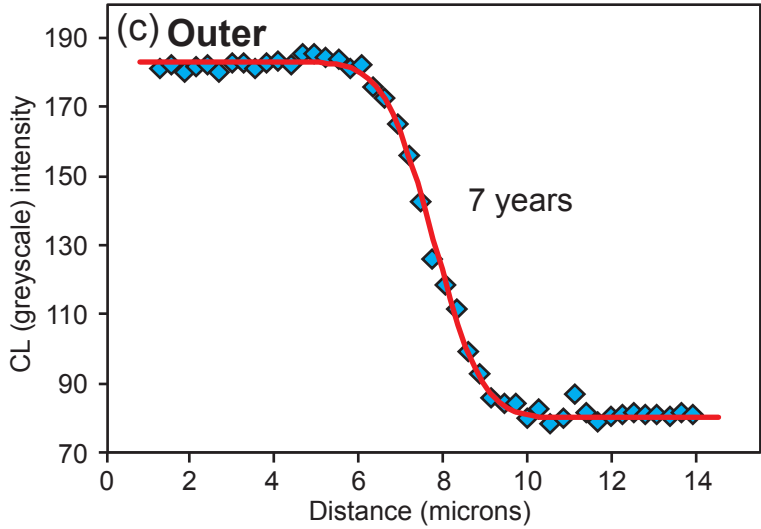
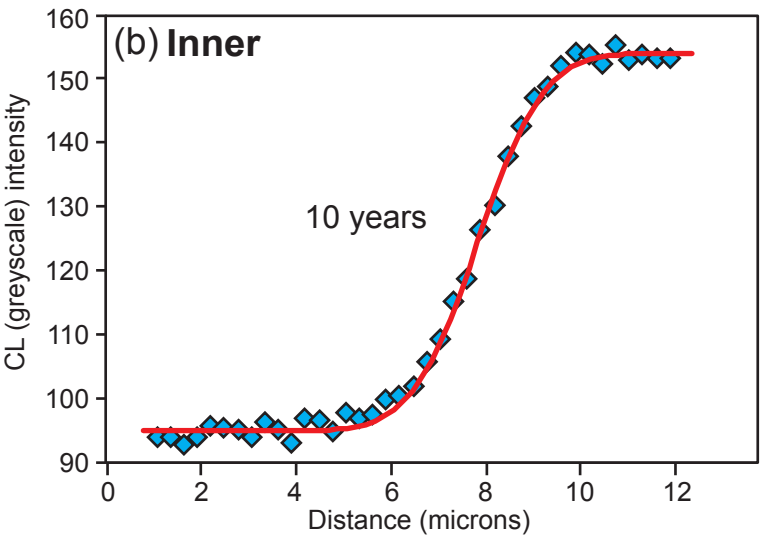
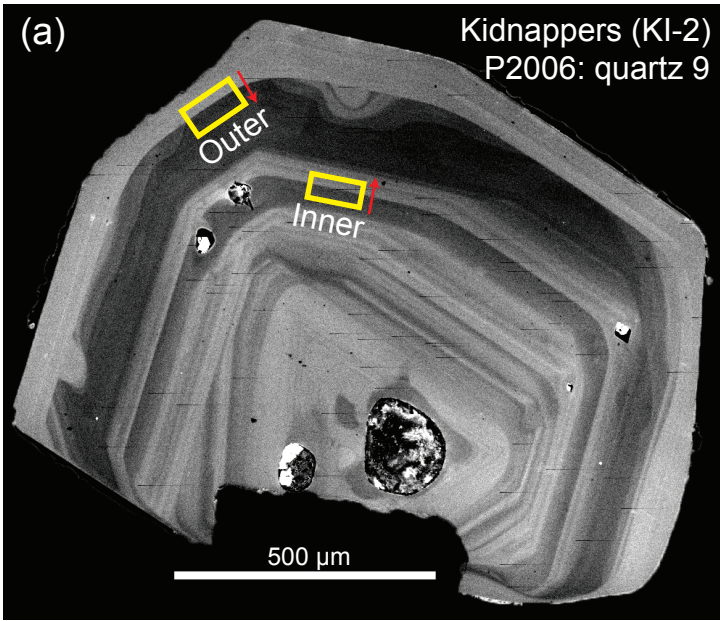


Figure 6
[Click here to download Figure: Fig. 6.pdf](#)

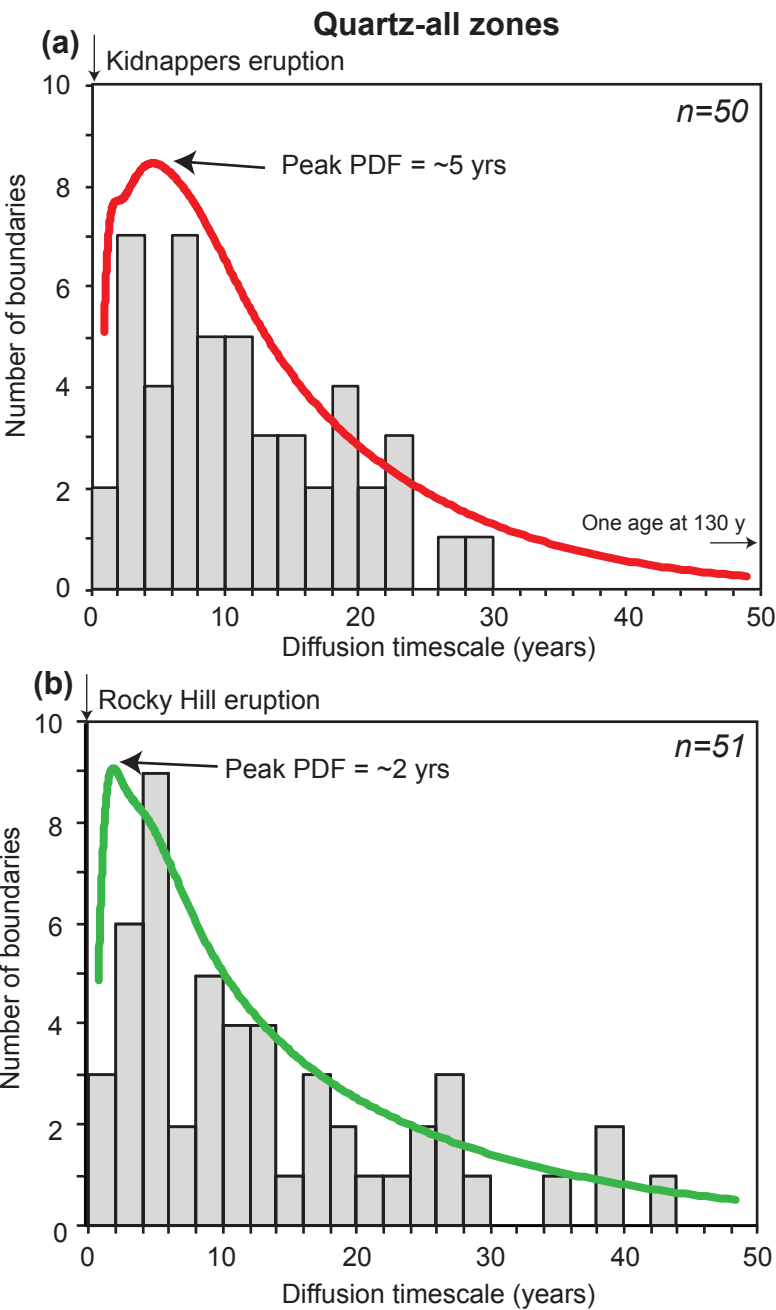


Figure 7
[Click here to download Figure: Fig. 7.pdf](#)

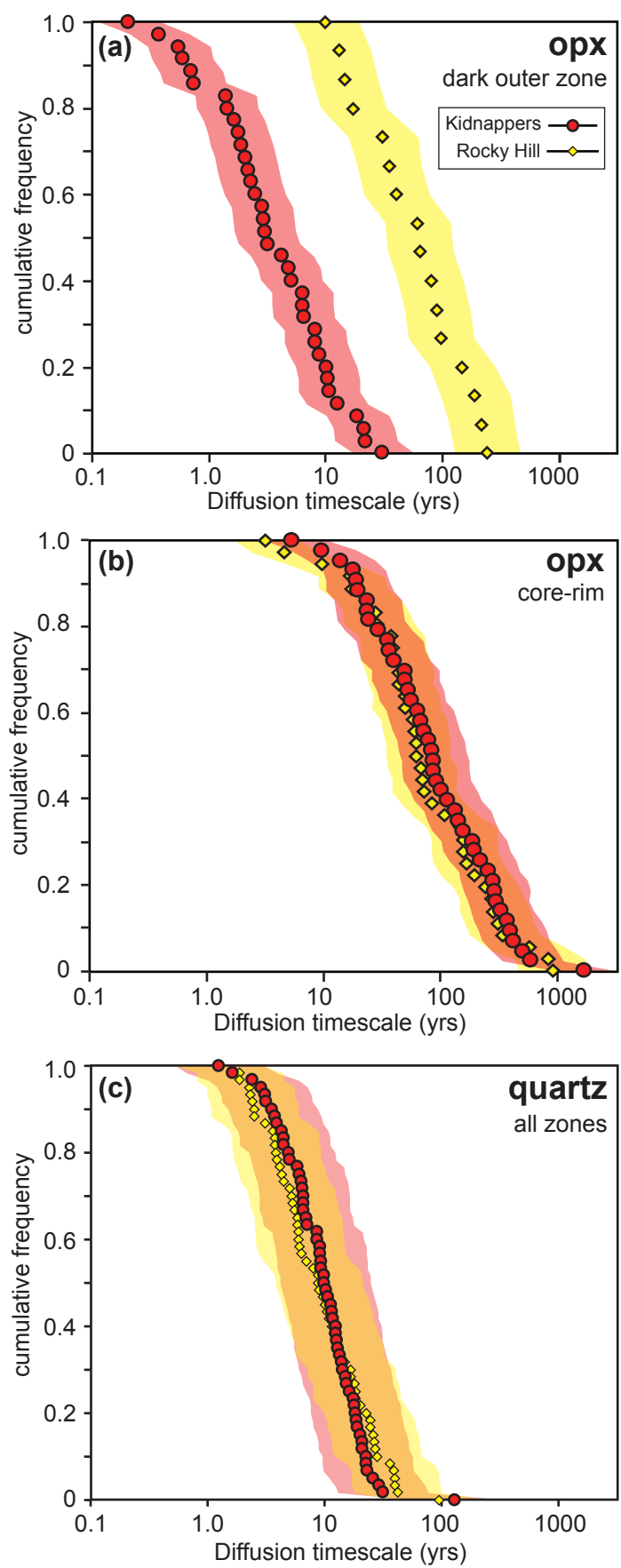


Figure 8
Click here to download Figure: Fig. 8.pdf
Fig. 8

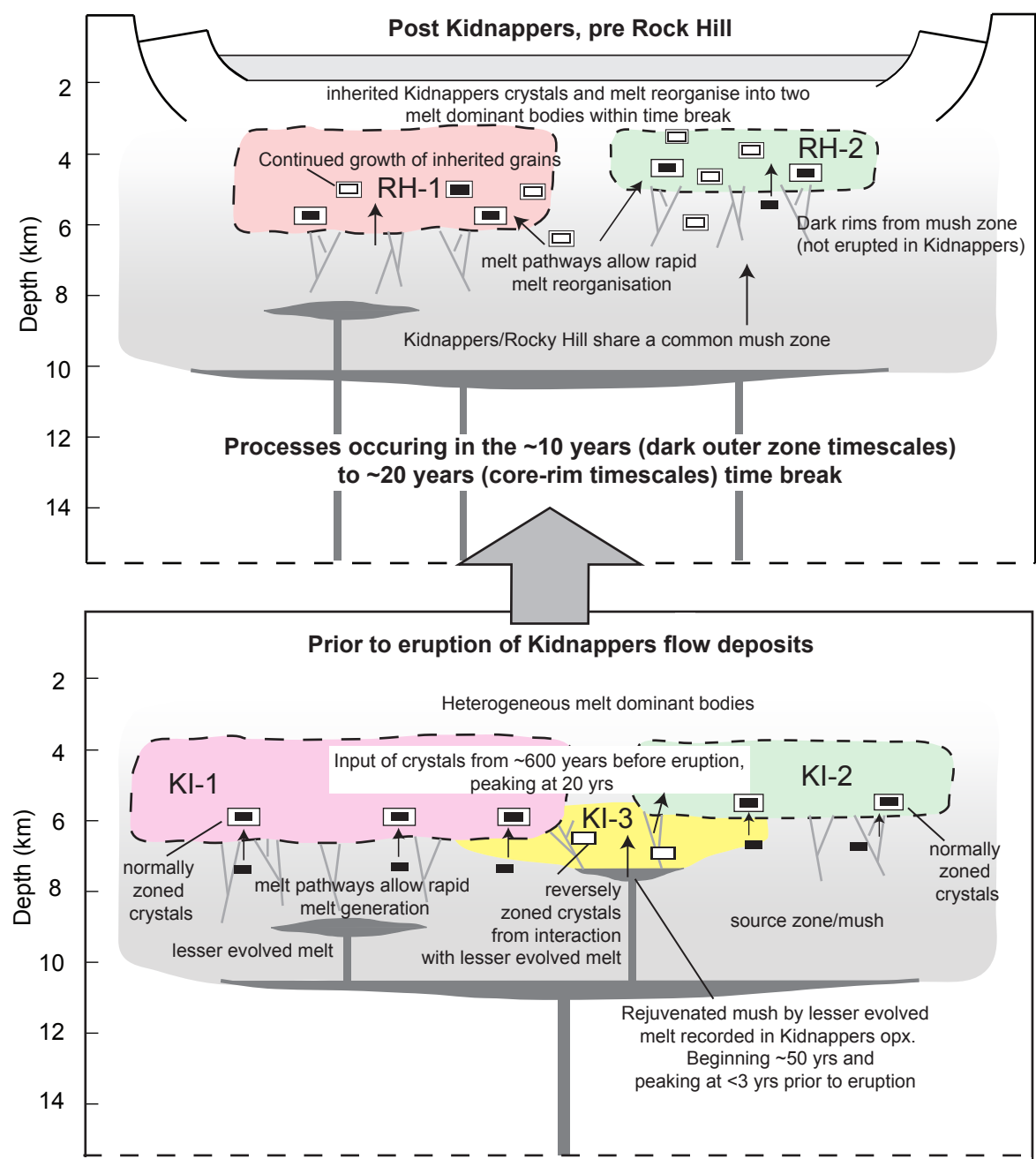


Table 1. Summary of orthopyroxene textural populations.

Groups and samples	Temperature	fO_2 (ΔNNO)	Normal	Reverse	Unzoned	Patchy	Dark outer
Kidnappers							
KI-3 (low-SiO₂) P1655, P17XX	820 °C	0.1	34.0 %	7.6 %	51.4 %	6.9 %	41.0 %
KI-1 (mid-SiO₂) P1646, P1649, P2011	785 °C	0.0	53.1 %	3.1 %	42.2 %	1.6 %	5.5 %
KI-2 (high-SiO₂) P1607, P1609, P2006, P2015	780 °C	0.2	76.2 %	1.2 %	15.2 %	7.3 %	2.4 %
Rocky Hill							
RH-1 (normal) P2000, P2029, P2042, P2049, P2050	795 °C	0.1	54.7 %	6.6 %	38.1 %	0.6 %	13.2 %
RH-2 (high SiO₂) P2046	765 °C	0.0	94.3 %	1.1 %	4.6 %	0.0 %	1.1 %

Temperatures presented were used to calculate orthopyroxene diffusive timescales from each compositional group from the Kidnappers and Rocky Hill.

Table 2. Summary of quartz textural populations.

Groups and samples	Temperature	Dark rim	Light rim	No significant change
Kidnappers				
KI-2 (P2006)	780 °C	80 %	7 %	13 %
Rocky Hill				
RH-1 (P2050)	795 °C	19.5 %	61 %	19.5 %

Textural classification in based on CL intensities. Temperatures presented were used to calculate quartz diffusive timescales.